A Bayesian luminescence chronology for the Bawa Yawan Rock Shelter at the Central Zagros Mountains (Western Iran)

Maryam Heydari, Guillaume Guérin, Saman Heydari-Guran

A Bayesian luminescence chronology for the Bawa Yawan Rock Shelter at the Central Zagros Mountains (Western Iran)

Maryam Heydari [a,b,*], Guillaume Guérin[c], Saman Heydari-Guran[d,e]

[a]Institute of Earth and Environmental Sciences, University of Freiburg, Albertstr. 23b, 79104, Freiburg, Germany
[b]IRAMAT-CRP2A, UMR 5060, CNRS-Université Bordeaux Montaigne, Maison de l'archéologie, Esplanade des Antilles, 33607, Pessac Cedex, France
[c]Univ Rennes, CNRS, Géosciences Rennes, UMR 6118, 35000 Rennes, France
[d]Institute for Prehistoric Archaeology University of Cologne, Weyertal 125, 50931 Cologne, Germany
[e]Diyarmehr Institute for Palaeolithic Research, Kermanshah, Iran

*Corresponding author.
E-mail address: maryam.heydari@geologie.uni-freiburg.de (M. Heydari).

Abstract

Bawa Yawan Rock Shelter is one of the critical Palaeolithic sites discovered recently in the Central Zagros in Western Iran. The site exhibits a rich assemblage from the Middle Palaeolithic (Zagros Mousterian) to the Epipalaeolithic, and it discloses one Neanderthal canine tooth. The site stands out as one of the handfuls of Palaeolithic sites in the Central Zagros that contain human remains. Therefore, establishing a reliable chronology revealing the temporal period in which Neanderthals inhabited the region plays a significant role in our understanding of the human past in the region. We employed luminescence dating in combination with Bayesian modelling to improve the precision of the estimated ages. Our results indicate that the Middle Palaeolithic assemblages unearthed from geological layers GH3 to GH5 in the site fall in the [58-80] ka time frame (68% credible interval). More importantly, the Bayesian age for the layer containing the Neanderthal remains exhibited [65-71] ka (68%). This age contradicts the previous ^{14}C-based chronology. We argue that it is likely that the ^{14}C dates underestimate the timing of the Middle Palaeolithic industries at Bawa Yawan.

Furthermore, our study reveals the first luminescence age for the Epipalaeolithic in the Central Zagros, which is dated to [13–15] ka (68%).

Keywords: Luminescence dating; Bayesian modelling; Middle Palaeolithic; Epipalaeolithic; Neanderthals; Central Zagros

1 Introduction

The Central Zagros has long been the centre of attention for Palaeolithic studies in Western Iran. Recently, human fossil remains, although sparsely discovered, proved the presence of Neanderthals and Anatomically Modern Humans (AMHs) during the Middle and Upper Palaeolithic (Heydari-Guran et al., 2021a; Trinkaus et al., 2008; Trinkaus and Biglari, 2006; Tsanova, 2013; Zanolli et al., 2019). In addition, an abundance of caves and rock shelters preserving rich Middle-Upper to Epipalaeolithic assemblages distinguishes this area (Heydari-Guran and Ghasidian, 2020, 2017).

Notably, the Kermanshah Province, in Western Iran and its spectacular Bisotun Massif are renowned for encompassing several famous archaeological sites that have witnessed Palaeolithic cultures and were investigated in attempts to decipher them (Biglari, 2001). This brings our attention to the Bisotun (Hunter) cave, which was excavated by Coon in 1948, who uncovered one of the first Mousterian industries for this region (Biglari, 2001; Coon, 1951).

Later, Smith (1986) excavated another cave (Ghār-e Khar) representing the continued assemblages from the Middle, Upper to Epipalaeolithic (Shidrang et al., 2016). Mar-Tarik, Mar-Aftab, and Mar-Dodar caves were other key sites that opened doors to buried Mousterian culture in the Central Zagros in the Bisotun Massif (Biglari, 2001; Jaubert et al., 2009, 2006). Mar-Dodar, however, was marked since it renders assemblages associated with the Upper and Epipalaeolithic as well as the Mousterian industries (Biglari, 2001). Another exceptional discovery in Kermanshah Province occurred in the Warwasi Rock Shelter, which was first excavated in 1961 (Braidwood et al., 1961; Hole and Flannery, 1968) and represented remarkably continuous assemblages associated with the Middle, Upper to Epipalaeolithic culture (Olszewski, 1993; Olszewski and Dibble, 2006; Tsanova, 2013).

During the last decade, the new Palaeolithic research in the Kermanshah Region began in the framework of “Human evolution in the Zagros Mountains” (HEZM) including documenting new sites, conducting test excavations aimed at understanding the history of various hominin occupations and their behaviour from the Lower Palaeolithic until the beginning of the Neolithic (Heydari-Guran and Ghasidian, 2020, 2017). Recent excavations in the Gelimgoush Cave presented the Upper Palaeolithic layer dated back to ca. 40 ka as well as the Bronze Age occupations (Heydari-Guran et al., 2021b).

In close vicinity of Kermanshah, in the Lurestan Province, the sites of Pasangar (Bazgir et al., 2014; Hole and Flannery, 1968) and Yafteh (Hole and Flannery, 1968; Otte et al., 2011) are best-known examples for the Upper Palaeolithic culture of the Central Zagros. In addition, Gilvaran and Kaldar caves (Bazgir et al., 2017, 2014) represented the rich Middle Palaeolithic technology below the lithic artefacts associated with the Upper Palaeolithic.

The aforementioned sites were only some of the Palaeolithic excavations’ history in the Central Zagros, and new explorations are in progress to get a grip on the bigger picture of Late Palaeolithic cultures in the area. Overall, the need for a reliable time frame in which prehistoric humans lived has risen by increasing the number of excavations and unfolding the buried cultural affinities of the Central Zagros. The necessity for chronological studies in the Central Zagros seems even more significant since absolute dates are only available for a few sites (Bazgir et al., 2017; Becerra-Valdivia et al., 2017; Otte et al., 2011).

Importantly, chronological studies play a major role in solving the key questions as to whether one culture (e.g., Zagros Aurignacian, Late Upper Palaeolithic) is rooted or locally evolved from a former one (e.g., Zagros Mousterian) which has been invariably engaged the archaeologists (Olszewski and Dibble, 2006; Tsanova, 2013). More crucially, the time of Neanderthal and AMH

arrivals into the Central Zagros, the period during which they may have coexisted in the area, and finally, the precise timing of Neanderthal disappearance can be determined through reliable dating techniques.

Our study attempts to improve our knowledge of the timing of Late Palaeolithic human occupations in the Central Zagros. Our focus will be on Kermanshah Province and one of the latest Palaeolithic discoveries in the Rock Shelter of Bawa Yawan (Fig. 1). This site stands out from several prior findings in this region since it provided direct evidence of Neanderthal occupation (canine tooth) in this region. The archaeological record recovered from the site noteworthily rendered assemblages associated with the Middle, Upper, and Epipalaeolithic cultures. This sequence was recently dated using the ^{14}C method, suggesting that the Neanderthal occupied the site between 43,600 a cal. BP and 41,500 a cal. BP (Heydari-Guran et al., 2021a).

However, previous studies showed that ^{14}C dates for Middle-Upper Palaeolithic assemblages could be underestimated due to the limited time range of the method (e.g., Higham, 2011; Higham et al., 2009; Wood et al., 2013; Zhang et al., 2022; Zilhão et al., 2021) and frequent contamination (e.g., Devièse et al., 2021). As such, due to the importance of the site for the region, it seems vital that other dating methods with a longer age range (covering the Middle Palaeolithic) are applied to the site to establish an independent chronology. The method we employed at Bawa Yawan is luminescence dating. This technique has been coupled with archaeological studies across the globe and successfully ascertained the time frame from Epipalaeolithic to the Lower-Middle Palaeolithic (e.g., Daura et al., 2021; Demeter et al., 2022; Godfrey-Smith et al., 2003; Grine et al., 2007; Groucutt et al., 2021; Guo et al., 2015; Heydari et al., 2022; Iovita et al., 2012; Malinsky-Buller et al., 2016; Sun et al., 2010; Wintle, 2008).

Our study aims to establish the first luminescence-based chronology for the Bawa Yawan Rock Shelter and compare the new dates with the earlier study using the ^{14}C dating. Furthermore, we provide the first absolute luminescence age representing the Epipalaeolithic culture for the Central Zagros.

Notably, Bayesian modelling tailored to luminescence data is employed to improve the precision of the ages by incorporating the stratigraphic relationships between the geological layers. We test whether Bayesian luminescence chronologies confirm the radiocarbon dates or if they contradict the previous study.

1.1 Bawa Yawan Rock Shelter: Geological layers and archaeological findings

The abundance of vast plains with sufficient water supply provided by the Gamasiab and Dinevar Rivers amid the Central Zagros foothills likely rendered a suitable environment for prehistoric humans (Biglari, 2001). This seems to be the main reason why the Kermanshah Province encompasses a vast suite of prehistoric sites. Based on geological and geomorphological records, Heydari-Guran and Ghasidian (2017) categorised these sites into four key subzones. Their preliminary survey identified 265 sites offering human industries attributable to the Middle to Epipalaeolithic time. These field investigations revealed the importance of rock shelters in Palaeolithic excavations, as the buried assemblages are most likely to be preserved from erosion and weathering.

The Bawa Yawan Rock Shelter was first discovered in 2009 due to a field survey in which many lithic artefacts were observed following nearby road constructions (Heydari-Guran and Ghasidian, 2017). The site sits right below the southern slope of limestone cliffs with an elevation of 50 m in the Nawdarwan Valley, where about 50 more palaeolithic sites have been identified (Heydari-Guran et al., 2021a).

Later, during 2016-2018, the site was subject to systematic excavations disclosing in situ assemblages mainly attributed to the Middle and Upper Palaeolithic. The excavations opened two main trenches on the west and the east of the cliffs, with an area of 14 m^2 and 6 m^2, respectively (cf. Fig. 3 in Heydari-Guran et al., 2021a).

The archaeological findings in Bawa Yawan originated from five geological horizons (GH) separated due to their sedimentary properties, including their colour and granulometry (Fig. 2) (Heydari-Guran et al., 2021a). The topmost layer with a thickness of 50 cm is GH1, which is distinguished from other geological layers by its dark reddish-brown colour. The evidence of an erosional discordance separated this layer from the ones below. This layer offers no Palaeolithic findings, only some modern materials (Heydari-Guran et al., 2021a).

GH2 is extended in reddish-brown colour over 80-95 cm thickness. This deposit consists of particles ranging from clay to larger pebbles and cobbles. The archaeological findings from this layer are categorised into the Middle, Upper, and Epipalaeolithic. Fragmented faunal remains, such as birds, *Bovidae*, and *caprinae*, were also obtained from this layer (Heydari-Guran et al., 2021a).

Layer GH3 is visible at about 95 cm depth, and its dull and dark reddish-brown colour separates it from other layers. The layer is rich in calcium carbonate mixed with some pebbles. It comprises fewer lithic artefacts than other layers, mainly attributed to the Middle Palaeolithic (using the Levallois flaking technology). GH4 spans 65 cm and appears in a light reddish-brown colour. The number of cobbles here increases significantly compared to the other layers (Heydari-Guran et al., 2021a). On the other hand, the number of lithic artefacts associated with the Middle Palaeolithic markedly drops in this layer.

The last excavated layer (GH5) is 150 cm thick and is of dark reddish-brown colour due to the abundance of iron oxide. The grain size ranged from silt and sand grains to pebbles (i.e. limestones from the wall shelter). The layer offers the richest Palaeolithic assemblages (associated with the Zagros Mousterian) compared to the other overlying layers. In addition, it contains burnt bones and faunal remains. Unlike the other layers, the number of faunal remains in GH5 is abundant. Faunal species, including *Bovidae, Antilopinae*, and *Equidae* have been identified in this layer (Heydari-Guran et al., 2021a)

2 Material and methods

Optically Stimulated Luminescence dating (OSL; Huntley et al., 1985) was applied to quartz and polymineral grains to determine when grains were exposed to sunlight. This timing is assumed to be equivalent to the burial time of the sediment (i.e., minerals), including deposited archaeological findings, which are associated with the dates of human occupations in the rock shelter.

Luminescence dating benefits from the ability of particular minerals (e.g., quartz and feldspar) to absorb the dose administered to them due to the natural decay of radionuclides, mainly ^{238}U, ^{232}Th, and ^{40}K. In the laboratory, we estimate the recorded dose in the mineral by measuring the natural and regenerated luminescence signals. This estimated dose is an equivalent dose (D_e) since it estimates the dose minerals have received during their burial period. In addition, the environmental dose rate (i.e. the dose per unit time) is approximated and allows for ascertaining sediment age by dividing the equivalent dose (D_e) by the dose rate.

To estimate the ages of the sediments at Bawa Yawan, we took six samples from GH2 to GH5. From each layer, only one sample was extracted except for GH5, from which three samples were taken using opaque tubes. For simplicity, henceforth, sample names are preceded by

"BaYa" for Bawa Yawan. The first sample (BaYa1) was taken outside the trench from the uppermost GH2 outcrop, where Epipalaeolithic lithic artefacts were identified. Samples BaYa2, BaYa3, BaYa4 and BaYa5 were taken inside the trench from the profile wall. The last sample BaYa6 was taken from the bed of the trench.

2.1 Sample preparation

Sample preparation for luminescence dating followed standard procedures (Preusser et al., 2008). Samples were prepared under subdued orange light conditions (ca 589 nm, sodium vapour lamp) appropriate for luminescence samples. Wet sieving was performed on the samples to extract grains ranging from 20 µm to 41 µm. This grain-size range was selected since no sufficient material was available in larger grain sizes (see Fig. S1 in supplementary material). The samples were then treated with HCl (10 %) until no more reaction was observed, and this was followed by soaking in HCl (35 %) for one hour to dissolve any remaining carbonates. The samples were treated with H_2O_2 (30%) for 48 hours to eliminate organic materials. We kept a part of the so-prepared samples (polymineral) for infrared light-stimulated luminescence (IRSL) measurements. The other part was soaked with a mixture of hexafluorosilicic acid (H_2SiF_6, 37%) plus nitric acid (HNO_3, 68%) (a solution of 90% of hexafluorosilicic acid plus 10% of nitric acid) for one week to obtain purified quartz grains. This procedure was followed by another wash in HCl (15 %) overnight to remove Ca-fluorides. Finally, wet sieving was applied again to discard grains smaller than the target grain size.

2.2 Instrumentation and source calibration

We used two Freiberg Instruments lexsyg SMART TL/OSL systems (Richter et al., 2015) for our measurements. The system used for the D_e estimation of the quartz grains (called S2) facilitated five blue LEDs (458 Δ 10 nm, max. 70 mW cm^{-2}) and five infrared LEDs (850 Δ 3 nm, max. 300 mW cm^{-2}). The power densities were set to 40 mW cm^{-2} (blue stimulation) and 100 mW cm^{-2} (infrared stimulation) during continuous wave (CW) stimulation. Luminescence signal of quartz was detected through a UV filter set (Hoya U340, 2.5 mm, and Delta BP 365/50 EX) in front of a Hamamatsu H7360-02 photomultiplier tube (PMT). For the D_e estimation of the polymineral fraction, the system (called S1) used five infrared LEDs (850 Δ 3 nm, max. 300 mW cm^{-2}), which were set to 100 mW cm^{-2} during CW stimulation. Luminescence signal of polymineral was detected using a Schott BG 39, 3 mm in conjunction with an AHF-BL HC 414/46 and a Schott NG 11, 1 mm filter.

We specifically calibrated the $^{90}Sr/^{90}Y$ sources for our samples due to the small grain size (20–41 µm). We used grains from sample BaYa3 for the calibration with the polymineral material and sample BaYa4 for the calibration with the quartz grains. The samples were first bleached using a solar simulator (Hönle UVA CUBE400) following the procedure applied for dose recovery test (see the detail below) and then irradiated with an external ^{137}Cs gamma-source in the laboratory of Gif-sur-Yvette (Laboratoire des Sciences du Climat et de l'Environnement, France, cf. Tribolo et al., 2019). The samples received doses of 106 Gy and 212 Gy, respectively. We measured the given dose using a single-aliquot regenerative dose (SAR) protocol (Murray and Wintle, 2000) with the same setup as our measurements (see below). The result showed that the luminescence readers S1 and S2 delivered dose rates of ca 11.3 Gy min^{-1} and ca 8.6 Gy min^{-1} on polymineral and quartz grains from the grain size fraction 20–41 µm, respectively (see Sec. S1).

For the measurements, several hundred grains, either quartz or polymineral, were mounted on stainless-steel cups using silicone oil (1 mm spray mask). We measured 20–25 aliquots per sample for the polymineral and 37-40 aliquots for the quartz fractions.

2.3 Luminescence signal measurements

Luminescence signals from quartz and polymineral were measured separately to establish two series of ages for our samples. This approach was employed to gain additional information on the minerals' signal bleaching (resetting) history (Murray et al., 2012). In doing so, we can assess whether or not the complete signal resetting occurred before the deposition at the site, which is a key assumption for estimating an exact age. Below, we detail the signal measurements for both quartz and polymineral.

2.3.1 Quartz signal measurements

The blue OSL was used to determine the D_e through the SAR protocol (see Table S1 for protocol details).

The measured luminescence signal often combines several superimposed signals, while the fast-decaying signal shows several advantages for dating (Wintle and Murray, 2006). First, the domination of the fast decaying signal in Bawa Yawan samples was tested by comparing the shapes of the OSL signal of sample BaYa2 with the fast component dominated calibration quartz (Risø batch 90, Hansen et al., 2015) following the approach of Bos and Wallinga (2012). A preheat-plateau test was performed to monitor the dependency of the estimated D_e on the thermal treatments in the SAR protocol. In this test, a series of temperatures from 220 °C to 280 °C (20 °C increments) was applied to three samples (BaYa1, BaYa2, and BaYa5), and five aliquots were used to measure the D_e. The cut-heat was always set at 20 ˚C lower than the corresponding preheat temperature in each step. The temperature on a plateau was considered an appropriate temperature for the SAR protocol.

In addition, we carried out a dose-recovery test on two samples by measuring six aliquots for samples BaYa1 and BaYa2. The aliquots were first bleached for 100 s inside a Hönle UVACUBE 400 solar simulator to deplete the natural luminescence signal. This step was followed by a 10,000 s pause that allows for the decay of the 110 °C peak (Wintle and Murray, 2006). Then, the samples were bleached for a second time for 100 s to empty charges in the fast component, potentially transferred from the shallow 110 °C trap during the pause. Finally, samples BaYa1 and BaYa2 received a beta dose of 33 Gy and 149 Gy (close to their expected D_e values) inside the OSL reader, and the SAR protocol was applied to test whether the given dose could be satisfyingly recovered.

We used the initial channels 1-2 (first 0.2 s) for the signal stimulated with blue and subtracted the late background using channels 300–400 (last 10 s). The SAR protocol was applied to multi-grain aliquots of quartz to determine the equivalent dose (D_e). Four regenerative points, approximately 56 Gy, 112 Gy, 224 Gy, and 449 Gy, were used to construct the dose-response curves for samples BaYa2 to BaYa6, with a test dose of 56 Gy. A different setup was used for sample BaYa1 due to its lower D_e compared to other samples: regenerative doses of 14 Gy, 28 Gy, 56 Gy, and 112 Gy, with a test dose of 14 Gy. A single saturating exponential equation was used to fit the dose-response curves forced through the origin.

2.3.2 Polymineral signal measurements

The post-infrared infrared stimulated luminescence at 290 °C ($pIRIRSL_{290}$) was applied to the polymineral fraction to estimate the D_e. This signal was selected since it was proven that it

does not suffer from anomalous fading, or at least the signal loss is insignificant (Buylaert et al., 2012; Thiel et al., 2011; Thomsen et al., 2008). The protocol settings for this measurement were derived after Buylaert et al. (2012) (see Table S2 for the details of the setting).

We used four regenerative doses (19 Gy, 38 Gy, 76 Gy, and 152 Gy) with a test dose of 19 Gy to construct the dose-response curve for BaYa1. These regenerative doses were increased to 66 Gy, 133 Gy, 265 Gy, and 531 Gy, with a test dose of 66 Gy for samples BaYa2 to BaYa6. The single saturating exponential function was also used to fit the regenerative dose points to build up the dose-response curve, which passed through the origin.

The dose-recovery test was conducted on two samples (BaYa1 and BaYa2). The samples were bleached for 72 hours in the solar simulator, and then they received doses of 43 Gy and 170 Gy, respectively. The given dose was measured using the $pIRIRSL_{290}$ protocol with the test doses of ca 18 Gy and 64 Gy for BaYa1 and BaYa2, respectively.

2.4 Dose rate estimation

Radioactive nuclides of the U-series, the Th-series, and K emit alpha, beta particles, and gamma- rays. The contribution from every type of decay is estimated to approximate the environmental dose rate as a whole. The input from cosmic rays and the internal activities of K (10 ± 2%) after Smedley et al. (2012) and Rb Mejdahl (1987) for feldspar grains were also considered in the calculation.

We employed high-resolution, low-background gamma-ray spectrometry (Guibert and Schvoerer, 1991) to estimate the concentrations of U, Th, and K. This allows for approximating the amount of alpha-, beta- and gamma-dose rates separately.

In order to improve the accuracy of the beta and gamma-dose rates (derived from gamma-ray spectrometry), the sediment samples were sieved and separated in two series: less than 2 mm (series 1) and between 2 mm and 1 cm (series 2). Initially, the contribution of the beta dose rate was taken into account only from the particle size of less than 2 mm. However, recent studies argued that larger particles than 2 mm up to 1 cm in a heterogenous environment could also play a non-negligible part in beta-dose rate fraction (Martin, 2015; Tribolo et al., 2017). Therefore, the beta dose rates were determined using both series 1 and series 2 to better represent the contribution of this part.

The sediment samples were first powdered using a planetary mill before being sealed in plastic boxes of 12 cm^3 and stored before the measurements for at least three weeks. The equivalent U, Th, and K concentrations were obtained for both particle size series using gamma-ray spectrometry. The values from both series were then converted into dose rates using the conversion factors by Guérin et al. (2011). The alpha-dose rates were determined only based on the radionuclide concentrations of series 1.

To determine the beta dose rate, first, we estimated the beta dose rate for each series. Then, we calculated the weighted mean of both series using the relative weight of each fraction. This, in total, gives us the beta dose rate originating from particles smaller than 1 cm.

Martin (2015) showed that the true beta dose rate was always lying in a range somewhere between the contributions of <1 cm and <2 mm. Thus, the final beta dose rate was calculated using the average of fractions <1 cm and <2 mm (Martin, 2015; Tribolo et al., 2017), which represents the best estimate for the beta dose rate in this environment.

For the gamma dose rate, however, the contribution from the fraction <1 cm was considered. Although this approach would not give us the ideal estimate, it could improve the obtained value as it reflected grains larger than 2 mm (up to 1 cm).

The water content was measured after storing the sediment samples in an external furnace at 50˚C for around one week. These values ranged between 15 ± 6 % and 17 ± 7 %. Except for sample BaYa4, for which the value was 14 ± 5 %. We increased this value to 16 ± 6 % for consistency with the other two samples (BaYa5 and BaYa6) taken from the same unit (GH5). The obtained dose rates were then corrected for the water content (Aitken, 1985; Guérin and Mercier, 2012; Nathan and Mauz, 2008). The effect of the grain size-dependent attenuation for alpha and beta dose rates was corrected after Guérin et al. (2012) and Martin et al. (2014). We used the value of 0.03 ± 0.01 (OSL quartz, Mauz et al., 2006) and 0.09 ± 0.01 (mean of the values reported in Schmidt et al., 2018 for $pIRIR_{290}$ protocol) for the alpha-efficiency in order to determine the beta equivalent alpha dose rate contribution. The cosmic-dose rate was estimated from the geographic position and burial depth of each sample (Prescott and Hutton, 1994) using the function *calc_CosmicDoseRate()* in the (R Core Team, 2023) package 'Luminescence' (Kreutzer et al., 2023, 2012).

2.5 Bayesian chronology

Bayesian modelling was employed to improve the precision of each time frame using the R package "BayLum" (Christophe et al., 2023; Philippe et al., 2019). This modelling allows for including independent chronological information of the site, e.g., stratigraphic relationships, for reducing age uncertainties.

This model was applied to analyse quartz OSL signals and created posterior dose-response curves through a single saturating exponential function. Simultaneously, the Gaussian distribution was used to generate equivalent dose posterior probability for each sample, which, combined with the dose rate, led to the age probability distribution. We applied the function *SC_Ordered()* to include the stratigraphic constraints and improve the precision of obtained ages, as was displayed in an earlier study (Heydari et al., 2020). The systematic error was modelled by generating the theta matrix (Guérin et al., 2021).

3 Results

3.1 Quartz D_e

The perfect matching in the shape of the OSL signals of sample BaYa2 and the calibration quartz indicates that the fast-decaying component is dominating the OSL signal of sample BaYa2 (Fig. S2). The results of the preheat plateau test for samples BaYa1, BaYa2, and BaYa5 are illustrated in Fig. S3. We observed a plateau between 260 °C to 280 °C, 220 °C to 260 °C and 240 °C to 260 °C for samples BaYa1, BaYa2 and BaYa5, respectively. Based on this observation, a preheat temperature at 260 °C was selected for the measurement of the D_e of all samples.

Dose-recovery ratios for samples BaYa1 and BaYa2 were 1.03 ± 0.02 and 0.95 ± 0.04, respectively, which are in the acceptable range of 0.9−1.1. These ratios indicate that the parameters in the SAR protocol are appropriately adjusted for these samples.

The recuperation ratio after delivering a zero dose was consistently below 5 % of the natural signal. A repeat of the first regenerative dose point (recycling ratio) was used to monitor the sensitivity changes due to previous thermal treatments and irradiations. The means of recycling ratios for each sample ranged from 0.90 ± 0.05 to 0.95 ± 0.01, inferring its close consistency within 10 % of unity (Murray and Wintle, 2000). The possibility of contamination by feldspar grains was examined by using IR depletion ratio (Duller, 2003). This ratio was within 10 % of unity for all samples. Therefore, no significant evidence for feldspar

contamination was observed. Figure 3a illustrates the preheat TL curves, blue stimulated shine-down curves, and corresponding dose-response curves for sample BaYa4 as an example. The D_e values and their uncertainties (obtained using the software package "Analyst"; Duller, 2015) are quoted using the arithmetic mean and the standard error of the mean, which ranged from 34±1 Gy to 204±7 Gy for samples BaYa1 to BaYa6 (Table 3). The D_e distribution for sample BaYa4 is illustrated as an example using the Abanico plot (Fig. 4a) (Dietze et al., 2016).

Except for BaYa1, which was taken from the external outcrop at the top of the profile, the D_e values for BaYa2 to BaYa6 fall in the high dose range, between 139±3 Gy and 204±7 Gy. This means these values were obtained after projecting the sensitivity-corrected natural signal (L_n/T_n) onto the non-linear part of the dose-response curve. In such a circumstance, as was discussed in previous studies, the accuracy of the D_e estimate could be dubious, and D_e tends to be underestimated (e.g., Duller, 2007; Heydari and Guérin, 2018). To evaluate the accuracy of the obtained D_e for our samples, we first estimated the characteristic saturation dose value (D_0) through a single saturating exponential function for the last two samples with the largest D_e values. We constructed dose-response curves using regenerative points ranging from 36 Gy to 1224 Gy (in total 11 points). The results are shown in Fig. S4. The D_0 values for BaYa5 and BaYa6 were 117 Gy and 107 Gy, respectively. For both samples, the determined D_e values are lower than $2D_0$, justifying the estimate's accuracy (Wintle and Murray, 2006).

Nevertheless, Heydari and Guérin (2018) showed that applying Bayesian models to estimate D_e for samples lying in the non-linear part of the dose-response curve or close to saturation can lead to more accurate results. Thus, we applied the Bayesian modelling using Gaussian distribution and estimated D_e values for two samples (with the largest D_e values BaYa5 and BaYa6), which resulted in the [180-193] Gy and [190-214] Gy intervals (68% credible intervals), respectively. These ranges are consistent with the values obtained through the non-Bayesian approach within their uncertainties (195 ± 6 Gy for BaYa5 and 204 ± 7 Gy for BaYa6), indicating that D_e underestimation does not seem to be likely for this dataset.

3.2 Polymineral D_e

The first dose-recovery ratios were 0.97 ± 0.03, 0.94 ± 0.01 for samples BaYa1 and BaYa2 (each sample three aliquots). We then tried to modify the protocol by varying the test-dose values (Colarossi et al., 2018) to potentially improve the dose-recovery ratios (Wintle and Murray, 2006). We increased the value of the test dose from the 56 Gy used in the first test, to 85 Gy for BaYa2, which resulted in ratios of 0.83 ± 0.03. We also reduced the value of the test dose for this sample to 43 Gy, which led to 0.91 ± 0.07. Therefore, we selected the first protocol settings for our final measurements, which provided the most satisfactory result compared to the two other protocols.

Figure 3b displays preheat TL curves, infrared light-stimulated shine-down curves, and corresponding dose-response curves of the $pIRIR_{290}$ signal for sample BaYa4 as an example. The D_e for BaYa1 was 50 ± 1 Gy, and BaYa2 to BaYa6 ranged from 168 ± 3 Gy to 259 ± 8 Gy. The D_e values for all samples were estimated using the mean of the distribution, and the corresponding uncertainty was ascertained through the standard error of the mean. The Abanico plot was used to visualise the D_e distributions for sample BaYa4 as an example (Fig. 4b).

3.3 Does rate results

The equivalent concentrations of U, Th, and K are listed in Table 1 according to particle sizes (series 1 and 2).

The alpha-dose rates ranged from 0.12 ± 0.02 to 0.17 ± 0.02 Gy ka^{-1} for the quartz grains and from 0.37 ± 0.03 to 0.53 ± 0.04 Gy ka^{-1} for the polymineral fraction. Beta-dose rates were calculated using the concentrations from series 1 and 2, and they ranged from 1.26 ± 0.10 to 1.65 ± 0.14 Gy ka^{-1}. The gamma dose rates were also determined using series 1 and 2 concentrations ranging from 0.70 ± 0.02 to 0.86 ± 0.04 Gy ka^{-1}. The internal dose rate for feldspar accounted for 0.11 ± 0.03 Gy ka^{-1}, and the cosmic dose rates fell between 0.15 ± 0.02 Gy ka^{-1} to 0.24 ± 0.02 Gy ka^{-1}. The final dose rates for quartz and polymineral ranged from 2.26 ± 0.10 Gy ka^{-1} to 2.84 ± 0.15 Gy ka^{-1} and 2.62 ± 0.11 Gy ka^{-1} to 3.30 ± 0.15 Gy ka^{-1}, respectively. The beta and gamma dose rates contribute 55–58 % and 29–31% to the external dose rates. The alpha dose rates for quartz and polymineral were about 5–6 % and 14–16 % of their total dose rates.

3.3.1 Radioactive disequilibria

Disequilibrium in the U-decay chain can impact the accuracy of luminescence dating. This can happen under various environmental conditions in which intermediate radioactive products are transported mainly due to fluctuations in the groundwater system.

The chemical mobility of ^{226}Ra often causes disequilibrium in the U-decay chain. To examine whether this is the case in our sediments, the effective concertation of U was estimated using elements of ^{234}Th, ^{234m}Pa, and ^{234}U from the top of the chain (pre-^{226}Ra) and also from ^{214}Pb and ^{214}Bi at the bottom of the chain (post-^{226}Ra).

The concentrations of ^{238}U determined from the top of the U-decay chain range from 2.23 ± 0.10 ppm to 4.79 ± 0.15 ppm for series 1 and from 2.09 ± 0.09 ppm to 4.22 ± 0.11 ppm for series 2. The concentrations derived from the bottom of the chain of series 1 vary between 1.91 ± 0.03 ppm to 2.90 ± 0.03 ppm and from series 2 between 2.30 ± 0.03 ppm to 3.25 ± 0.03 ppm. To better visualise the disequilibria observed in these datasets, we determined the ratios by dividing the effective ^{238}U concentration from the pre-^{226}Ra and the post-^{226}Ra to ^{232}Th due to its immobility after (Guibert et al., 2009). These ratios for series 1 and 2, alongside the equilibrium line, are presented in Figure 5. As shown in this figure, the radioactive equilibrium is evidently discerned for series 2 for samples BaYa2 to BaYa6. Moreover, this figure depicts a typical plot of a series of samples that have undergone a recent arrival of ^{238}U after Guibert et al. (2009). According to this observation, the effective U concentrations were used only from the bottom part of the chain to minimise the impact of recent U arrival in the site for these samples.

3.4 Age results and Bayesian chronology

Luminescence ages are established for all six samples using quartz (blue OSL) and polymineral fraction ($pIRIRSL_{290}$). The OSL and $pIRIRSL_{290}$ ages for the BaYa1 sample were 14 ± 1 ka and 18 ± 1 ka, respectively. The $pIRIRSL_{290}$ age is older than the corresponding OSL age. An age gap is noticed below this sample where BaYa2 was taken. The luminescence-derived time frame for this sample based on quartz OSL and $pIRIRSL_{290}$ on polymineral exhibited 59 ± 3 ka and 61 ± 3 ka, respectively. Here, both time frames perfectly agree with one another within their uncertainties. The dating for sample BaYa3 from GH4 rendered 68 ± 4 ka and 64 ± 3 ka through OSL and $pIRIRSL_{290}$, again within uncertainties in good accordance between the two ages. For the layer beneath, GH5, quartz, and polymineral ages yielded 65 ± 4 ka, and 62 ± 3 ka,

448 respectively and thus show excellent consistency. The OSL and pIRIRSL$_{290}$ ages of the
449 lowermost sample were 69 ± 4 ka and 73 ± 4 ka for sample BaYa5 and 73 ± 5 ka and 79 ± 5 ka
450 for BaYa6, respectively. Again, the ages are consistent within uncertainties here, and BaYa6
451 seems slightly older than BaYa5, which follows the stratigraphic position in the profile (see
452 Sec. S1).
453 Figure 6 illustrates the Bayesian age probability distribution for the six samples using quartz
454 OSL data. The ages are reported in 68% and 95% credible intervals.
455 The youngest age resulted in [13-15] ka (68% credible interval). The age results for the
456 subsequence samples read BaYa2 [58-64] ka, BaYa3 [63-68] ka, BaYa4 [65-71] ka, BaYa5 [68-
457 74] ka, and BaYa6 [72-80] ka (all 68% credible interval). They follow the expected stratigraphic
458 order as they increase smoothly within the depth. The impact of stratigraphic constraints is
459 observed in the Bayesian chronology, and its incorporation into the modelling has reduced
460 the random error and resulted in age intervals of higher precision.

461 # 4 Discussion

462 ## 4.1 Reliability of the obtained luminescence ages

463 One of the main critical premises controlling the accuracy of luminescence age is the
464 complete resetting of the signal before the deposition. In this study, we benefited from the
465 quartz OSL and pIRIRSL$_{290}$ (on polymineral fraction) signals to probe whether the natural
466 dosimeters were fully reset before deposition and whether the estimated D_e carries a former
467 dose originating from an earlier stage of sedimentation.
468 It has been shown that the bleaching rate of quartz OSL is far (orders of magnitude) faster
469 than the pIRIRSL$_{290}$ signal (Murray et al., 2012). This means that if the quartz OSL and
470 pIRIRSL$_{290}$ ages are consistent, the possibility of incomplete bleaching of these natural
471 dosimeters is unlikely. In our data set, it is easily discerned that the ages based on these two
472 signals overlap within the uncertainties. Hence, we conclude that incomplete bleaching is not
473 a probable scenario at the Bawa Yawan Rock Shelter. The only exception for which no
474 overlapping is observed is sample BaYa1. This sample resulted in the youngest age range in
475 which the pIRIRSL$_{290}$ age of 17-19 ka is older than the OSL of 13-15 ka. It is known that the
476 pIRIRSL$_{290}$ signal often contains a residual dose that is hard to bleach and contributes to the
477 measured natural signal. The amount of the residual dose for well-bleached samples typically
478 ranges from 5-20 Gy after (Buylaert et al., 2011). Although these values cannot significantly
479 impact the larger D_e values, their contributions to the small D_e (as is the case for sample BaYa1)
480 can be considerable. The residual doses were calculated for all samples (except for BaYa3 and
481 BaYa4) using a simple assumption that polymineral and quartz ages for each sample should
482 lead to equal value. The obtained residual doses account for 7-21 Gy, consistent with Buylaert
483 et al. (2011). The pIRIRSL$_{290}$ ages are slightly younger than the quartz OSL for two samples,
484 BaYa3 and BaYa4. While they are not statistically distinguishable within uncertainty, the
485 insignificant fading rate reported for the pIRIRSL$_{290}$ signal (Thiel et al., 2011) could explain this
486 minor age discrepancy.
487 As a result, we conclude that the quartz OSL ages are more reliable, and Bayesian modelling
488 was only employed for this dataset. The central dose for each sample was estimated by
489 selecting the Gaussian distribution. The low range of overdispersion (Galbraith et al., 1999)
490 for all samples (7-24%, Table S3) combined with the D_e distributions display (Fig. 4) favour this
491 choice, and the average seems to be a reasonable representative value expressing the final
492 D_e for each sample.

In this study, aside from the sediment particles smaller than 2 mm, we included a higher range (up to 1 cm) to better estimate the beta dose rate. We used this procedure because Martin (2015) argued, supported by simulations of the heterogeneous environment, that the true beta dose rate emanated not only from the fine grains (less than 2 mm) but also from the larger grain size (smaller than 1 cm). Thus, the weighted mean according to the weight proportion of these two grain size distributions is the best quantity representing the beta dose rate. Nevertheless, estimating the gamma dose rate based on radionuclide concentrations originating only from particles less than 1 cm in a heterogeneous environment (like Bawa Yawan) does not seem like an ideal approximation. The presence of limestones, known to be low in radioactivity, could shift our gamma dose rate estimate towards the lower values. So, in that case, it is likely that our ages are underestimated. But despite that, it is important to take into account that the contribution of the beta dose rate in the final dose rate is much higher than the gamma dose rate (about two times), and this means that probable underestimation cannot be significant given the uncertainty.

We also benefited from the Bayesian modelling, which was developed specifically for OSL data and allowed for incorporating the stratigraphic relationships in the site. This combination improved the precision of the age range (up to ca 38% for the Bawa Yawan Rock Shelter), as already demonstrated for other Palaeolithic sites in Iran (Heydari, 2020; Heydari et al., 2021, 2020). While ^{14}C dates are available for the site, they were not combined with the OSL ages since it appears likely that they are underestimated.

4.2 Timing of Epi- and Middle Palaeolithic culture at the Bawa Yawan Rock Shelter

In the following, the obtained ages are reported within 68% credible intervals.

The youngest sample, BaYa1, was taken from the topmost GH2, where the lithic artefacts associated with Epipalaeolithic culture were unearthed. The Bayesian age interval resulted in [13-15] ka and rendered the first luminescence age for the Epipalaeolithic industries in the Central Zagros. This time frame is consistent with the ^{14}C date (13,400–13,300 a cal. BP) estimated at the Bawa Yawan for the Epi-palaeolithic (Heydari-Guran et al., 2021a). Moreover, it agrees in general with the temporal period of 23/22–11.5 ka cal. BP suggested for the Epipalaeolithic culture in the Levant (Bar-Yosef and Belfer-Cohen, 2010). Our estimation also aligns with the ^{14}C time frame established for the Epipalaeolithic in Iraqi Kurdistan in closer vicinity (ca 19,600–13,000 a cal. BP) (Asouti et al., 2020).

Below GH2, the OSL ages determined for GH3 to GH5 correspond to assemblages that were mainly attributed to the Middle Palaeolithic, known as Mousterian culture. The Bayesian chronology for these three layers falls between [58-80] ka.

This age range is in good accordance with the time frame of 50–75 ka ascertained for the latest Neanderthal fossils found in the Levant. (e.g., Bar-Yosef and Meignen, 2001; Been et al., 2017). Closer to the site, at Shanidar cave in the Northern Zagros, the preliminary output of luminescence chronological study suggested a period of 60-70 ka for the Neanderthal fossil discovered at the site (Pomeroy et al., 2020).

The human remains (Neanderthal canine tooth) unburied in GH5 is a spectacular finding in Bawa Yawan for which the Bayesian modelling resulted in [65-71] ka. While this age range is consistent with other chronological data established for the Neanderthal presence in the Levant or the North Zagros, it does not support the preliminary ^{14}C date for this layer. The ^{14}C date exhibited between 41,500-43,600 a cal. BP (Heydari-Guran et al., 2021a), which is younger than the luminescence age [65-71] ka obtained for this layer.

Therefore, we argue that the ^{14}C age for this layer is not within the reliable limits of radiocarbon dating and is most likely to underestimate the accurate timing of Neanderthal presence at Bawa Yawan. Thus, the Bayesian OSL estimate seems more justified. This conclusion is also supported by various studies in which ^{14}C dates (older than ca 30 ka) underestimated the target event, and luminescence ages seem to provide a more robust time frame due to its higher age range limit (e.g., Briant and Bateman, 2009; Long and Shen, 2015; Palstra et al., 2021; Song et al., 2015).

5 Conclusions

We established the luminescence-based chronology for the Palaeolithic site of Bawa Yawan in the Central Zagros. The ages were estimated using quartz OSL signal and $pIRIRSL_{290}$ on polymineral. The overall consistent ages indicated that the dosimeters were fully bleached before deposition, and the possibility of overestimation due to incomplete bleaching could be safely ruled out at the site.

We employed Bayesian modelling on OSL data and combined it with stratigraphic constraints to improve the precision of the chronology. Our chronological study revealed the first luminescence-based age for the Epipalaeolithic culture in the Central Zagros, which narrowed down to [13-15] ka (68% credible interval). Furthermore, the Bayesian chronology for GH3 to GH5 containing the Middle Palaeolithic assemblages yielded the range of [58-80] ka (68% credible interval). Notably, GH5 comprised the Neanderthal canine tooth, dated to [65-71] ka (68% credible interval). This age range is larger than the previously determined ^{14}C date for this layer and contradicts it.

Based on our study, we suggest caution in dating the Middle Palaeolithic assemblages with the ^{14}C method since it is likely that this method underestimates the temporal range of the event of interest. We argue that applying another dating method, like luminescence, with a higher age range is essential for this particular temporal period.

Author contributions

Maryam Heydari: Conceptualization, Methodology, Investigation, Writing - Original Draft, Review & Editing. **Saman Heydari-Guran**: Review & Editing, Visualization. **Guillaume Guérin**: Review & Editing, Funding acquisition.

Data availability

The data that support the findings of this study are available from the corresponding author, [maryam.heydari@geologie.uni-freiburg.de].

Declaration of competing interest

The authors declare no conflict of interest.

Acknowledgements

We are grateful for the thorough suggestions and comments provided by anonymous reviewers. This study was part of the PhD thesis of MH that was financed by the Laboratoire d'Excellence Sciences archéologiques de Bordeaux (LaScArBx), a programme supported by

the Agence Nationale de la Rerchere (ANR) – n°ANR-10-LABX-52. Chantal Tribolo is thanked for her support in running the measurements in 2019. During the manuscript preparation, MH received funding from the Alexander von Humboldt Foundation. Thanks go to Sebastian Kreutzer for his support with the map. We are grateful to the excavation team at the Bawa Yawan Rock Shelter, N. Hariri, E. Ghasidian, S. Asiabani, F. Azizi, N. Heydari, E. Fotohi and the people of the Yawan Village which strongly supported our research in the area.

590 **References**
591
592 Aitken, M.J., 1985. Thermoluminescence Dating. Academic Press, London.
593 Asouti, E., Baird, D., Kabukcu, C., Swinson, K., Martin, L., García-Suárez, A., Jenkins, E.,
594 Rasheed, K., 2020. The Zagros Epipalaeolithic revisited: New excavations and 14C
595 dates from Palegawra cave in Iraqi Kurdistan. PLoS ONE 15, e0239564.
596 https://doi.org/10.1371/journal.pone.0239564
597 Bar-Yosef, O., Belfer-Cohen, A., 2010. The Levantine Upper Palaeolithic and Epipalaeolithic,
598 in: South-Eastern Mediterranean Peoples Between 130,000 and 10,000 Years
599 Ago,edited by Garcea, E. A. A. Oxbow Books, pp. 144–167.
600 Bar-Yosef, O., Meignen, L., 2001. The Chronology of the Levantine Middle Palaeolithic Period
601 in Retrospect. bmsap 13. https://doi.org/10.4000/bmsap.6113
602 Bazgir, B., Ollé, A., Tumung, L., Becerra-Valdivia, L., Douka, K., Higham, T., van der Made, J.,
603 Picin, A., Saladié, P., López-García, J.M., Blain, H.-A., Allué, E., Fernández-García, M.,
604 Rey-Rodríguez, I., Arceredillo, D., Bahrololoumi, F., Azimi, M., Otte, M., Carbonell, E.,
605 2017. Understanding the emergence of modern humans and the disappearance of
606 Neanderthals: Insights from Kaldar Cave (Khorramabad Valley, Western Iran). Sci Rep
607 7, 43460. https://doi.org/10.1038/srep43460
608 Bazgir, B., Otte, M., Tumung, L., Ollé, A., Deo, S.G., Joglekar, P., López-García, J.M., Picin, A.,
609 Davoudi, D., van der Made, J., 2014. Test excavations and initial results at the Middle
610 and Upper Paleolithic sites of Gilvaran, Kaldar, Ghamari caves and Gar Arjene
611 Rockshelter, Khorramabad Valley, western Iran. Comptes Rendus Palevol 13, 511–525.
612 https://doi.org/10.1016/j.crpv.2014.01.005
613 Becerra-Valdivia, L., Douka, K., Comeskey, D., Bazgir, B., Conard, N.J., Marean, C.W., Ollé, A.,
614 Otte, M., Tumung, L., Zeidi, M., Higham, T.F.G., 2017. Chronometric investigations of
615 the Middle to Upper Paleolithic transition in the Zagros Mountains using AMS
616 radiocarbon dating and Bayesian age modelling. Journal of Human Evolution 109, 57–
617 69. https://doi.org/10.1016/j.jhevol.2017.05.011
618 Been, E., Hovers, E., Ekshtain, R., Malinski-Buller, A., Agha, N., Barash, A., Mayer, D.E.B.-Y.,
619 Benazzi, S., Hublin, J.-J., Levin, L., Greenbaum, N., Mitki, N., Oxilia, G., Porat, N., Roskin,
620 J., Soudack, M., Yeshurun, R., Shahack-Gross, R., Nir, N., Stahlschmidt, M.C., Rak, Y.,
621 Barzilai, O., 2017. The first Neanderthal remains from an open-air Middle Palaeolithic
622 site in the Levant. Sci Rep 7, 2958. https://doi.org/10.1038/s41598-017-03025-z
623 Biglari, F., 2001. Recent Finds of Paleolithic Period from Bisitun, Central Western Zagros
624 Mountains. Iranian Journal of Archaeology and History 28, 50–60.
625 Bos, A.J.J., Wallinga, J., 2012. How to visualize quartz OSL signal components. Radiation
626 Measurements 47, 752–758. https://doi.org/10.1016/j.radmeas.2012.01.013
627 Braidwood, R.J., Howe, B., Reed, C.A., 1961. The Iranian Prehistoric Project: New problems
628 arise as more is learned of the first attempts at food production and settled village
629 life. Science 133, 2008–2010.
630 Briant, R.M., Bateman, M.D., 2009. Luminescence dating indicates radiocarbon age
631 underestimation in late Pleistocene fluvial deposits from eastern England: A CROSS-
632 COMPARISON OF RADIOCARBON AND LUMINESCENCE DATING. J. Quaternary Sci. 24,
633 916–927. https://doi.org/10.1002/jqs.1258
634 Buylaert, J.-P., Jain, M., Murray, A.S., Thomsen, K.J., Thiel, C., Sohbati, R., 2012. A robust
635 feldspar luminescence dating method for Middle and Late Pleistocene sediments:

636 Feldspar luminescence dating of Middle and Late Pleistocene sediments. Boreas 41,
637 435–451. https://doi.org/10.1111/j.1502-3885.2012.00248.x
638 Buylaert, J.P., Thiel, C., Murray, A.S., Vandenberghe, D.A.G., Yi, S., Lu, H., 2011. IRSL and post-
639 IR IRSL residual doses recorded in modern dust samples from the Chinese Loess
640 Plateau. Geochronometria 38, 432–440. https://doi.org/10.2478/s13386-011-0047-0
641 Christophe, C., Philippe, A., Kreutzer, S., Guérin, G., Baumgarten, F.H., 2023. BayLum:
642 Chronological Bayesian Models Integrating Optically Stimulated Luminescence and
643 Radiocarbon Age Dating.
644 Colarossi, D., Duller, G.A.T., Roberts, H.M., 2018. Exploring the behaviour of luminescence
645 signals from feldspars: Implications for the single aliquot regenerative dose protocol.
646 Radiation Measurements 109, 35–44.
647 https://doi.org/10.1016/j.radmeas.2017.07.005
648 Coon, C.S., 1951. Coon, C. S.: Cave explorations in Iran, 1949. University Museum, University
649 of Pennsylvania, Philadelphia.
650 Daura, J., Sanz, M., Demuro, M., Arnold, L.J., Costa, A.M., Moreno, J., da Conceição Freitas,
651 M., Lopes, V., Égüez, N., Hoffmann, D.L., Benson, A., Cabanes, D., García-Targa, J.,
652 Fullola, J.M., 2021. A new chronological framework and site formation history for Cova
653 del Gegant (Barcelona): Implications for Neanderthal and Anatomically Modern
654 Human occupation of NE Iberian Peninsula. Quaternary Science Reviews 270, 107141.
655 https://doi.org/10.1016/j.quascirev.2021.107141
656 Demeter, F., Zanolli, C., Westaway, K.E., Joannes-Boyau, R., Duringer, P., Morley, M.W.,
657 Welker, F., Rüther, P.L., Skinner, M.M., McColl, H., Gaunitz, C., Vinner, L., Dunn, T.E.,
658 Olsen, J.V., Sikora, M., Ponche, J.-L., Suzzoni, E., Frangeul, S., Boesch, Q., Antoine, P.-
659 O., Pan, L., Xing, S., Zhao, J.-X., Bailey, R.M., Boualaphane, S., Sichanthongtip, P.,
660 Sihanam, D., Patole-Edoumba, E., Aubaile, F., Crozier, F., Bourgon, N., Zachwieja, A.,
661 Luangkhoth, T., Souksavatdy, V., Sayavongkhamdy, T., Cappellini, E., Bacon, A.-M.,
662 Hublin, J.-J., Willerslev, E., Shackelford, L., 2022. A Middle Pleistocene Denisovan
663 molar from the Annamite Chain of northern Laos. Nat Commun 13, 2557.
664 https://doi.org/10.1038/s41467-022-29923-z
665 Devièse, T., Abrams, G., Hajdinjak, M., Pirson, S., De Groote, I., Di Modica, K., Toussaint, M.,
666 Fischer, V., Comeskey, D., Spindler, L., Meyer, M., Semal, P., Higham, T., 2021.
667 Reevaluating the timing of Neanderthal disappearance in Northwest Europe. Proc.
668 Natl. Acad. Sci. U.S.A. 118, e2022466118. https://doi.org/10.1073/pnas.2022466118
669 Dietze, M., Kreutzer, S., Burow, C., Fuchs, M.C., Fischer, M., Schmidt, C., 2016. The abanico
670 plot: Visualising chronometric data with individual standard errors. Quaternary
671 Geochronology 31, 12–18. https://doi.org/10.1016/j.quageo.2015.09.003
672 Duller, G.A.T., 2015. The Analyst software package for luminescence data: overview and
673 recent improvements. Ancient TL 33, 35–42.
674 Duller, G.A.T., 2007. Assessing the error on equivalent dose estimates derived from single
675 aliquot regenerative dose measurements. Ancient TL 25, 15–24.
676 Duller, G.A.T., 2003. Distinguishing quartz and feldspar in single grain luminescence
677 measurements. Radiation Measurements 37, 161–165.
678 https://doi.org/10.1016/S1350-4487(02)00170-1
679 Galbraith, R.F., Roberts, R.G., Laslett, G.M., Yoshida, H., Olley, J.M., 1999. Optical dating of
680 single and multiple grains of quartz from Jinmium Rock Shelter, Northern Australia:
681 Part I, experimental design and statistical models. Archaeometry 41, 339–364.
682 https://doi.org/10.1111/j.1475-4754.1999.tb00987.x

683 Godfrey-Smith, D.I., Vaughan, K.B., Gopher, A., Barkai, R., 2003. Direct luminescence
684 chronology of the Epipaleolithic Kebaran site of Nahal Hadera V, Israel.
685 Geoarchaeology 18, 461–475. https://doi.org/10.1002/gea.10073
686 Grine, F.E., Bailey, R.M., Harvati, K., Nathan, R.P., Morris, A.G., Henderson, G.M., Ribot, I.,
687 Pike, A.W.G., 2007. Late Pleistocene Human Skull from Hofmeyr, South Africa, and
688 Modern Human Origins. Science 315, 226–229.
689 https://doi.org/10.1126/science.1136294
690 Groucutt, H.S., White, T.S., Scerri, E.M.L., Andrieux, E., Clark-Wilson, R., Breeze, P.S.,
691 Armitage, S.J., Stewart, M., Drake, N., Louys, J., Price, G.J., Duval, M., Parton, A., Candy,
692 I., Carleton, W.C., Shipton, C., Jennings, R.P., Zahir, M., Blinkhorn, J., Blockley, S., Al-
693 Omari, A., Alsharekh, A.M., Petraglia, M.D., 2021. Multiple hominin dispersals into
694 Southwest Asia over the past 400,000 years. Nature 597, 376–380.
695 https://doi.org/10.1038/s41586-021-03863-y
696 Guérin, G., Lahaye, C., Heydari, M., Autzen, M., Buylaert, J.-P., Guibert, P., Jain, M., Kreutzer,
697 S., Lebrun, B., Murray, A.S., Thomsen, K.J., Urbanova, P., Philippe, A., 2021. Towards
698 an improvement of optically stimulated luminescence (OSL) age uncertainties:
699 modelling OSL ages with systematic errors, stratigraphic constraints and radiocarbon
700 ages using the R package BayLum. Geochronology 3, 229–245.
701 https://doi.org/10.5194/gchron-3-229-2021
702 Guérin, G., Mercier, N., 2012. Preliminary insight into dose deposition processes in
703 sedimentary media on a scale of single grains: Monte Carlo modelling of the effect of
704 water on the gamma dose rate. Radiation Measurements 47, 541–547.
705 https://doi.org/10.1016/j.radmeas.2012.05.004
706 Guérin, G., Mercier, N., Adamiec, G., 2011. Dose-rate conversion factors: update. Ancient TL
707 29, 5–8.
708 Guérin, G., Mercier, N., Nathan, R., Adamiec, G., Lefrais, Y., 2012. On the use of the infinite
709 matrix assumption and associated concepts: A critical review. Radiation
710 Measurements 47, 778–785. https://doi.org/10.1016/j.radmeas.2012.04.004
711 Guibert, P., Lahaye, C., Bechtel, F., 2009. The importance of U-series disequilibrium of
712 sediments in luminescence dating: A case study at the Roc de Marsal Cave (Dordogne,
713 France). Radiation Measurements 44, 223–231.
714 https://doi.org/10.1016/j.radmeas.2009.03.024
715 Guibert, P., Schvoerer, M., 1991. TL dating: Low background gamma spectrometry as a tool
716 for the determination of the annual dose. International Journal of Radiation
717 Applications and Instrumentation. Part D. Nuclear Tracks and Radiation
718 Measurements 18, 231–238. https://doi.org/10.1016/1359-0189(91)90117-Z
719 Guo, Y.-J., Li, B., Zhang, J.-F., Roberts, R.G., 2015. Luminescence-based chronologies for
720 Palaeolithic sites in the Nihewan Basin, northern China: First tests using newly
721 developed optical dating procedures for potassium feldspar grains. Journal of
722 Archaeological Science: Reports 3, 31–40.
723 https://doi.org/10.1016/j.jasrep.2015.05.017
724 Hansen, V., Murray, A., Buylaert, J.-P., Yeo, E.-Y., Thomsen, K., 2015. A new irradiated quartz
725 for beta source calibration. Radiation Measurements 81, 123–127.
726 https://doi.org/10.1016/j.radmeas.2015.02.017
727 Heydari, M., 2020. Applying Bayesian models to improve luminescence-based chronologies
728 of Middle to Upper Palaeolithic sites in Iran. https://hal.science/tel-03367658/.

729 Heydari, M., Guérin, G., 2018. OSL signal saturation and dose rate variability: Investigating the
730 behaviour of different statistical models. Radiation Measurements 120, 96–103.
731 https://doi.org/10.1016/j.radmeas.2018.05.005
732 Heydari, M., Guérin, G., Kreutzer, S., Jamet, G., Kharazian, M.A., Hashemi, M., Nasab, H.V.,
733 Berillon, G., 2020. Do Bayesian methods lead to more precise chronologies? 'BayLum'
734 and a first OSL-based chronology for the Palaeolithic open-air site of Mirak (Iran).
735 Quaternary Geochronology 59, 101082.
736 https://doi.org/10.1016/j.quageo.2020.101082
737 Heydari, M., Guérin, G., Sirakov, N., Fernandez, P., Ferrier, C., Guadelli, A., Leblanc, J.-C.,
738 Taneva, S., Sirakova, S., Guadelli, J.-L., 2022. The last 30,000 to 700,000 years ago:
739 Unravelling the timing of human settlement for the Palaeolithic site of Kozarnika.
740 Quaternary Science Reviews 291, 107645.
741 https://doi.org/10.1016/j.quascirev.2022.107645
742 Heydari, M., Guérin, G., Zeidi, M., Conard, N.J., 2021. Bayesian luminescence dating at Ghār-
743 e Boof, Iran, provides a new chronology for Middle and Upper Paleolithic in the
744 southern Zagros. Journal of Human Evolution 151, 102926.
745 https://doi.org/10.1016/j.jhevol.2020.102926
746 Heydari-Guran, S., Benazzi, S., Talamo, S., Ghasidian, E., Hariri, N., Oxilia, G., Asiabani, S., Azizi,
747 F., Naderi, R., Safaierad, R., Hublin, J.-J., Foley, R.A., Lahr, M.M., 2021a. The discovery
748 of an in situ Neanderthal remain in the Bawa Yawan Rockshelter, West-Central Zagros
749 Mountains, Kermanshah. PLoS ONE 16, e0253708.
750 https://doi.org/10.1371/journal.pone.0253708
751 Heydari-Guran, S., Douka, K., Higham, T., Münzel, S.C., Deckers, K., Hourshid, S., Naderi, R.,
752 Asiabani, S., Ghasidian, E., 2021b. Early Upper Palaeolithic occupation at Gelimgoush
753 cave, Kermanshah; West-Central Zagros mountains of Iran. Journal of Archaeological
754 Science: Reports 38, 103050. https://doi.org/10.1016/j.jasrep.2021.103050
755 Heydari-Guran, S., Ghasidian, E., 2020. Late Pleistocene hominin settlement patterns and
756 population dynamics in the Zagros Mountains: Kermanshah region. Archaeological
757 Research in Asia 21, 100161. https://doi.org/10.1016/j.ara.2019.100161
758 Heydari-Guran, S., Ghasidian, E., 2017. The MUP Zagros Project: tracking the Middle–Upper
759 Palaeolithic transition in the Kermanshah region, west-central Zagros, Iran. Antiquity
760 91, e2. https://doi.org/10.15184/aqy.2016.261
761 Higham, T., 2011. European Middle and Upper Palaeolithic radiocarbon dates are often older
762 than they look: problems with previous dates and some remedies. Antiquity 85, 235–
763 249. https://doi.org/10.1017/S0003598X00067570
764 Higham, T., Brock, F., Peresani, M., Broglio, A., Wood, R., Douka, K., 2009. Problems with
765 radiocarbon dating the Middle to Upper Palaeolithic transition in Italy. Quaternary
766 Science Reviews 28, 1257–1267. https://doi.org/10.1016/j.quascirev.2008.12.018
767 Hole, F., Flannery, K.V., 1968. The Prehistory of Southwestern Iran: A Preliminary Report.
768 Proceedings of the Prehistoric Society 33, 147–206.
769 Huntley, D.J., Godfrey-Smith, D.I., Thewalt, M.L.W., 1985. Optical dating of sediments. Nature
770 313, 105–107. https://doi.org/10.1038/313105a0
771 Iovita, R., Fitzsimmons, K., Dobos, A., Hambach, U., Hilgers, A., Zander, A., 2012. Dealul Guran:
772 Evidence for Lower Palaeolithic (MIS 11) occupation of the Lower Danube loess
773 steppe. Antiquity 86(334), 973–989. https://doi.org/10.1017/S0003598X00048195
774 Jaubert, J., Biglari, F., Bordes, J.-G., Bruxelles, L., Mourre, V., Shidrang, S., Naderi, R., Alipour,
775 S., 2006. New Research on Paleolithic of Iran: Preliminary Report of 2004 Iranian-

776 French Joint Mission. Iranian Center for Archaeological Research, Tehran, Iran,
777 Archaeological Re- ports 17–26.
778 Jaubert, J., Biglari, F., Mourre, V., Bruxelles, L., Shidrang, S., Naderi, R., Mashkour, M.,
779 Maureille, B., Quinif, Y., Rendu, W., Laroulandie, V., 2009. The Middle Paleolithic
780 occupation of Mar-Tarik, a new Zagros Mousterian site in Bisotun massif (Kerman-
781 shah, Iran), in: Iran Paleolithic, Le Paléolithique d'Iran, edited by Otte, M., Biglari, F.,
782 and Jaubert, J. Bar International Series 7–27.
783 Kreutzer, S., Burow, C., Dietze, M., Fuchs, M., Schmidt, C., Fischer, M., Friedrich, J.,
784 Mercier, N., Philippe, A., Riedesel, S., Autzen, M., Mittelstrass, D., Gray, H.,
785 Galharret, J., 2023. Luminescence: Comprehensive Luminescence Data Analysis. R
786 package version 0.9.23. https://CRAN.R-project.org/package=Luminescence.
787
788 Kreutzer, S., Schmidt, C., Fuchs, Margret, Dietze, M., Fischer, M., Fuchs, Markus, 2012.
789 Introducing an R package for luminescence dating analysis. Ancient TL 30, 1–8.
790
791 Long, H., Shen, J., 2015. Underestimated 14C-based chronology of late Pleistocene high lake-
792 level events over the Tibetan Plateau and adjacent areas: Evidence from the Qaidam
793 Basin and Tengger Desert. Sci. China Earth Sci. 58, 183–194.
794 https://doi.org/10.1007/s11430-014-4993-2
795 Malinsky-Buller, A., Barzilai, O., Ayalon, A., Bar-Matthews, M., Birkenfeld, M., Porat, N., Ron,
796 H., Roskin, J., Ackermann, O., 2016. The age of the Lower Paleolithic site of Kefar
797 Menachem West, Israel—Another facet of Acheulian variability. Journal of
798 Archaeological Science: Reports 10, 350–362.
799 https://doi.org/10.1016/j.jasrep.2016.10.010
800 Martin, L., 2015. Caractérisation et modélisation d'objets archéologiques en vue de leur
801 datation par des méthodes paléo-dosimétriques. Simulation des paramètres
802 dosimétriques sous Geant4. Ph.D. Dissertation. Université Bordeaux Montaigne.
803 Martin, L., Mercier, N., Incerti, S., 2014. Geant4 simulations for sedimentary grains in infinite
804 matrix conditions: The case of alpha dosimetry. Radiation Measurements 70, 39–47.
805 https://doi.org/10.1016/j.radmeas.2014.09.003
806 Mejdahl, 1987. Internal radioactivity in quartz and feldspar grains. Ancient TL 5, 10–17.
807 Murray, A.S., Thomsen, K.J., Masuda, N., Buylaert, J.P., Jain, M., 2012. Identifying well-
808 bleached quartz using the different bleaching rates of quartz and feldspar
809 luminescence signals. Radiation Measurements 47, 688–695.
810 https://doi.org/10.1016/j.radmeas.2012.05.006
811 Murray, A.S., Wintle, A.G., 2000. Luminescence dating of quartz using an improved single-
812 aliquot regenerative-dose protocol. Radiation Measurements 32, 57–73.
813 https://doi.org/10.1016/S1350-4487(99)00253-X
814 Nathan, R.P., Mauz, B., 2008. On the dose-rate estimate of carbonate-rich sediments for
815 trapped charge dating. Radiation Measurements 43, 14–25.
816 https://doi.org/10.1016/j.radmeas.2007.12.012
817 Olszewski, D.I., 1993. The Late Baradostian occupation at Warwasi rockshelter, Iran, in: The
818 Paleolithic Prehistory of the Zagros-Taurus, edited by Olszewski, D. I. and Dibble, H.
819 The University Museum of Archaeology and Anthropology. University of Pennsylvania,
820 Philadelphia 186–206.
821 Olszewski, D.I., Dibble, H.L., 2006. To be or not to be Aurignacian: The Zagros Upper
822 Paleolithic, in: Towards a Definition of the Aurignacian, Proceedings of the Sympoisum

held in Lisbon, Portugal, June 25-30, 2002, edited by Bar-Yosef, O. and Zilhão, J., pp. 355–373, Instituto Português de Arqueologia, 2006. Instituto Português de Arqueologia, 355–373.
Otte, M., Shidrang, S., Zwyns, N., Flas, D., 2011. New radiocarbon dates for the Zagros Aurignacian from Yafteh cave, Iran. Journal of Human Evolution 61, 340–346. https://doi.org/10.1016/j.jhevol.2011.05.011
Palstra, S.W.L., Wallinga, J., Viveen, W., Schoorl, J.M., van den Berg, M., van der Plicht, J., 2021. Cross-comparison of last glacial radiocarbon and OSL ages using periglacial fan deposits. Quaternary Geochronology 61, 101128. https://doi.org/10.1016/j.quageo.2020.101128
Philippe, A., Guérin, G., Kreutzer, S., 2019. BayLum - An R package for Bayesian analysis of OSL ages: An introduction. Quaternary Geochronology 49, 16–24. https://doi.org/10.1016/j.quageo.2018.05.009
Pomeroy, E., Bennett, P., Hunt, C.O., Reynolds, T., Farr, L., Frouin, M., Holman, J., Lane, R., French, C., Barker, G., 2020. New Neanderthal remains associated with the 'flower burial' at Shanidar Cave. Antiquity 94, 11–26. https://doi.org/10.15184/aqy.2019.207
Prescott, J.R., Hutton, J.T., 1994. Cosmic ray contributions to dose rates for luminescence and ESR dating: Large depths and long-term time variations. Radiation Measurements 23, 497–500. https://doi.org/10.1016/1350-4487(94)90086-8
Preusser, F., Degering, D., Fuchs, M., Hilgers, A., Kadereit, A., Klasen, N., Krbetschek, M., Richter, D., Spencer, J.Q.G., 2008. Luminescence dating: basics, methods and applications. E&G Quaternary Sci. J. 57, 95–149. https://doi.org/10.3285/eg.57.1-2.5
R Core Team, 2023. R: A language and environment for statistical computing. http://www. R-project.org/.
Richter, D., Richter, A., Dornich, K., 2015. Lexsyg smart — a luminescence detection system for dosimetry, material research and dating application. Geochronometria 42, 202–209. https://doi.org/10.1515/geochr-2015-0022
Shidrang, S., Biglari, F., Bordes, J.-G., Jaubert, J., 2016. CONTINUITY AND CHANGE IN THE LATE PLEISTOCENE LITHIC INDUSTRIES OF THE CENTRAL ZAGROS: A TYPO-TECHNOLOGICAL ANALYSIS OF LITHIC ASSEMBLAGES FROM GHAR-E KHAR CAVE, BISOTUN, IRAN. Arheol. ètnogr. antropol. Evrazii 44, 27–38. https://doi.org/10.17746/1563-0110.2016.44.1.027-038
Smedley, R.K., Duller, G.A.T., Pearce, N.J.G., Roberts, H.M., 2012. Determining the K-content of single-grains of feldspar for luminescence dating. Radiation Measurements 47, 790–796. https://doi.org/10.1016/j.radmeas.2012.01.014
Smith, P.E.L., 1986. Paleolithic archaeology in Iran. The American Institute of Iranian Studies Monograph 1. Philadelphia (PA), The University Museum.
Song, Y., Lai, Z., Li, Y., Chen, T., Wang, Y., 2015. Comparison between luminescence and radiocarbon dating of late Quaternary loess from the Ili Basin in Central Asia. Quaternary Geochronology 30, 405–410. https://doi.org/10.1016/j.quageo.2015.01.012
Sun, X., Mercier, N., Falgueres, C., Bahain, J.-J., Despriee, J., Bayle, G., Lu, H., 2010. Recuperated optically stimulated luminescence dating of middle-size quartz grains from the Palaeolithic site of Bonneval (Eure-et-Loir, France). Quaternary Geochronology 5, 342–347. https://doi.org/10.1016/j.quageo.2009.05.004

Thiel, C., Buylaert, J.-P., Murray, A., Terhorst, B., Hofer, I., Tsukamoto, S., Frechen, M., 2011. Luminescence dating of the Stratzing loess profile (Austria) – Testing the potential of an elevated temperature post-IR IRSL protocol. Quaternary International 234, 23–31. https://doi.org/10.1016/j.quaint.2010.05.018

Thomsen, K.J., Murray, A.S., Jain, M., Bøtter-Jensen, L., 2008. Laboratory fading rates of various luminescence signals from feldspar-rich sediment extracts. Radiation Measurements 43, 1474–1486. https://doi.org/10.1016/j.radmeas.2008.06.002

Tribolo, C., Asrat, A., Bahain, J.-J., Chapon, C., Douville, E., Fragnol, C., Hernandez, M., Hovers, E., Leplongeon, A., Martin, L., Pleurdeau, D., Pearson, O., Puaud, S., Assefa, Z., 2017. Across the Gap: Geochronological and Sedimentological Analyses from the Late Pleistocene-Holocene Sequence of Goda Buticha, Southeastern Ethiopia. PLoS ONE 12, e0169418. https://doi.org/10.1371/journal.pone.0169418

Tribolo, C., Kreutzer, S., Mercier, N., 2019. How reliable are our beta-source calibrations? Ancient TL 37, 1–10.

Trinkaus, E., Biglari, F., 2006. Middle Paleolithic Human Remains from Bisitun Cave, Iran. paleo 32, 105–111. https://doi.org/10.3406/paleo.2006.5192

Trinkaus, E., Biglari, F., Mashkour, M., Monchot, H., Reyss, J.-L., Rougier, H., Heydari, S., Abdi, K., 2008. Late Pleistocene human remains from Wezmeh Cave, western Iran. Am. J. Phys. Anthropol. 135, 371–378. https://doi.org/10.1002/ajpa.20753

Tsanova, T., 2013. The beginning of the Upper Paleolithic in the Iranian Zagros. A taphonomic approach and techno-economic comparison of Early Baradostian assemblages from Warwasi and Yafteh (Iran). Journal of Human Evolution 65, 39–64. https://doi.org/10.1016/j.jhevol.2013.04.005

Wintle, A.G., 2008. FIFTY YEARS OF LUMINESCENCE DATING. Archaeometry 50, 276–312. https://doi.org/10.1111/j.1475-4754.2008.00392.x

Wintle, A.G., Murray, A.S., 2006. A review of quartz optically stimulated luminescence characteristics and their relevance in single-aliquot regeneration dating protocols. Radiation Measurements 41, 369–391. https://doi.org/10.1016/j.radmeas.2005.11.001

Wood, R.E., Barroso-Ruíz, C., Caparrós, M., Jordá Pardo, J.F., Galván Santos, B., Higham, T.F.G., 2013. Radiocarbon dating casts doubt on the late chronology of the Middle to Upper Palaeolithic transition in southern Iberia. Proc. Natl. Acad. Sci. U.S.A. 110, 2781–2786. https://doi.org/10.1073/pnas.1207656110

Zanolli, C., Biglari, F., Mashkour, M., Abdi, K., Monchot, H., Debue, K., Mazurier, A., Bayle, P., Le Luyer, M., Rougier, H., Trinkaus, E., Macchiarelli, R., 2019. A Neanderthal from the Central Western Zagros, Iran. Structural reassessment of the Wezmeh 1 maxillary premolar. Journal of Human Evolution 135, 102643. https://doi.org/10.1016/j.jhevol.2019.102643

Zhang, J.-F., Hou, Y.-M., Guo, Y.-J., Rui, X., Wang, Z.-H., Yang, Z.-M., Liu, Y., Zhen, Z.-M., Hu, Y., Zhou, L.-P., 2022. Radiocarbon and luminescence dating of the Wulanmulun site in Ordos, and its implication for the chronology of Paleolithic sites in China. Quaternary Geochronology 72, 101371. https://doi.org/10.1016/j.quageo.2022.101371

Zilhão, J., Angelucci, D.E., Arnold, L.J., Demuro, M., Hoffmann, D.L., Pike, A.W.G., 2021. A revised, Last Interglacial chronology for the Middle Palaeolithic sequence of Gruta da Oliveira (Almonda karst system, Torres Novas, Portugal). Quaternary Science Reviews 258, 106885. https://doi.org/10.1016/j.quascirev.2021.106885

Figure captions:

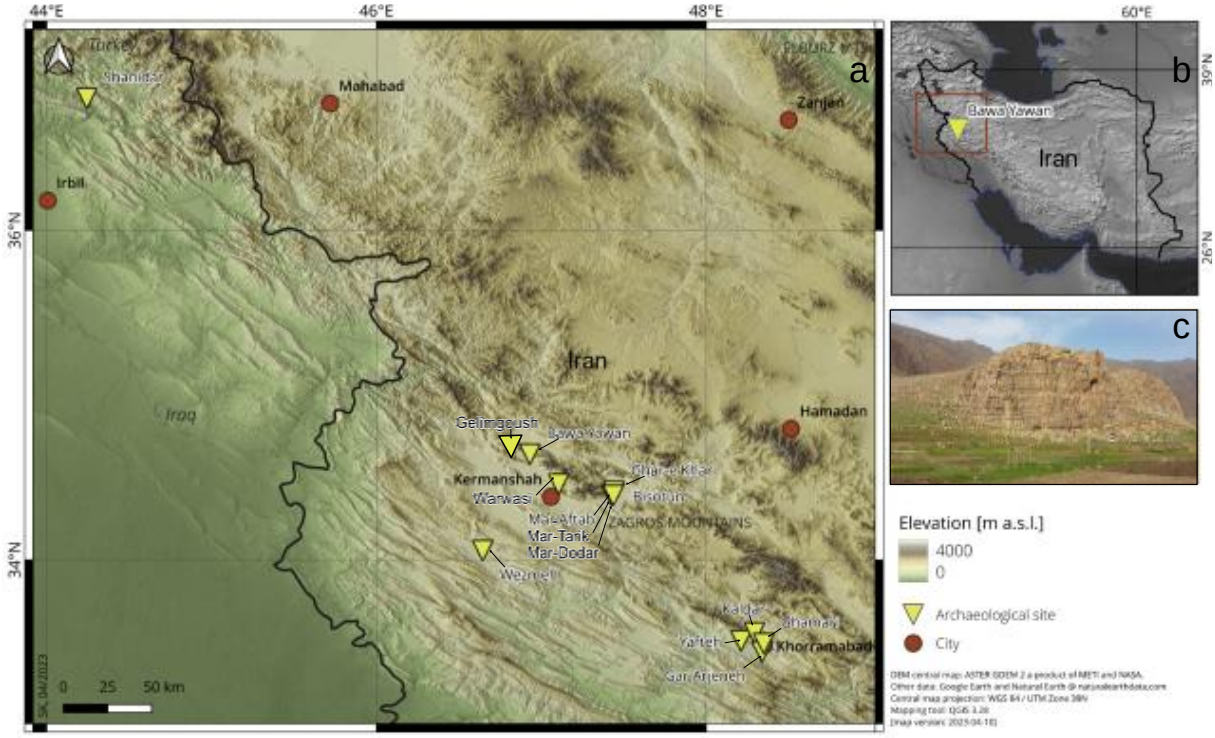

Figure 1. Study area of Bawa Yawan. The central map shows the important Palaeolithic sites close to Kermanshah city (a). The upper-right map shows the map of Iran, including the studied site in Western Iran (b). The photo displays the Bawa Yawan rock shelter (limestone cliffs) on the north-eastern valley terrace (c).

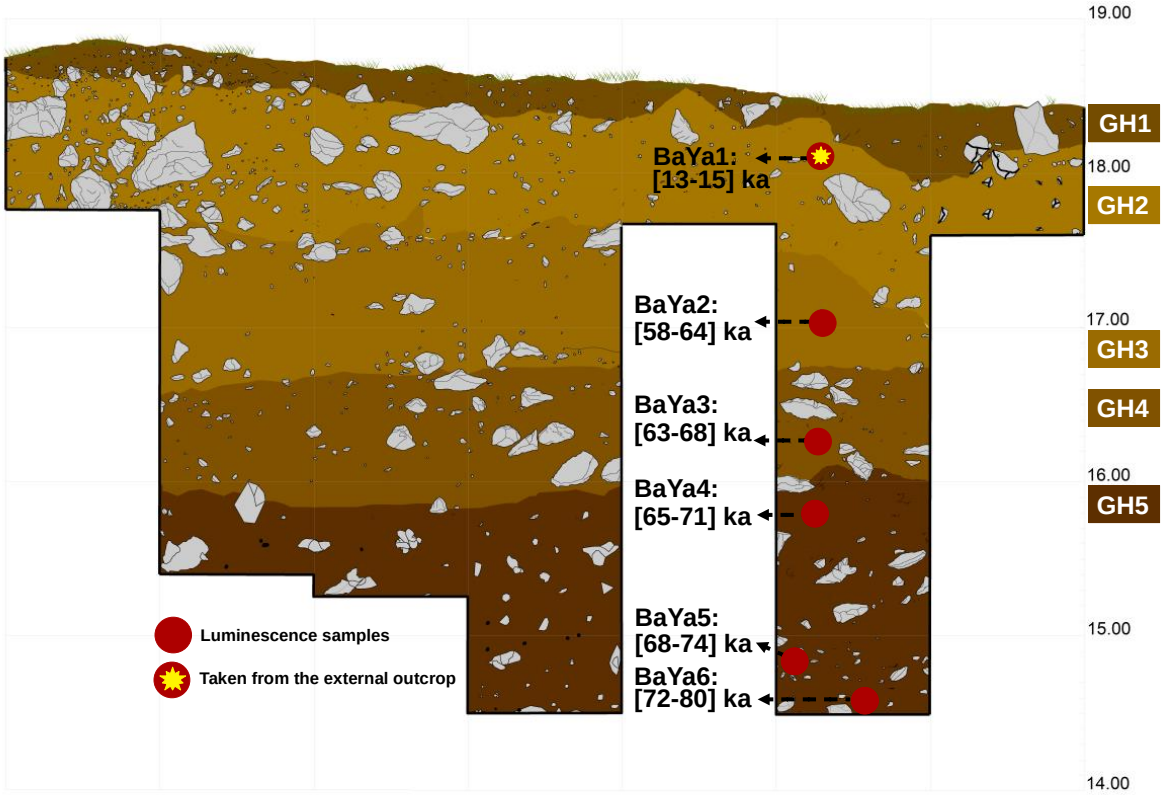

Figure 2. Profile sketch of the western trenches below the limestone cliffs. Five geological horizons (GH1 to GH5) are distinguishable, and Bayesian OSL ages for the samples are presented.

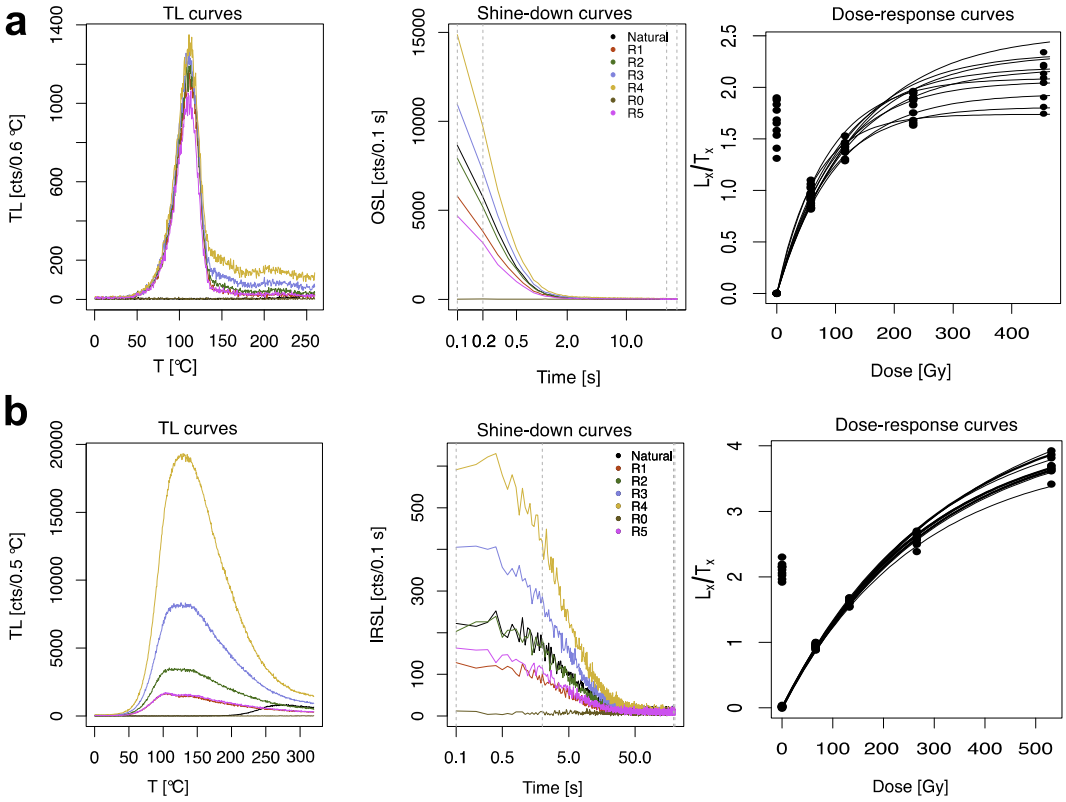

Figure 3. Typical TL preheat curves, shine-down curves, and typical dose-response curves for blue OSL (a) and pIRIRSL$_{290}$ (b) for sample BaYa4.

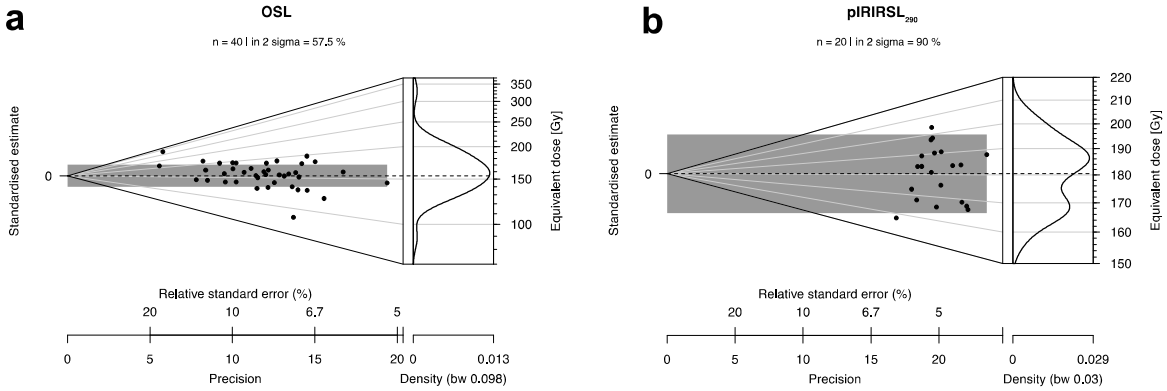

Figure 4. D_e distributions based on the OSL (a) and pIRIRSL$_{290}$ (b) signals for sample BaYa4 using the Abanico plot. The arithmetic average was used to estimate the central D_e for both distributions.

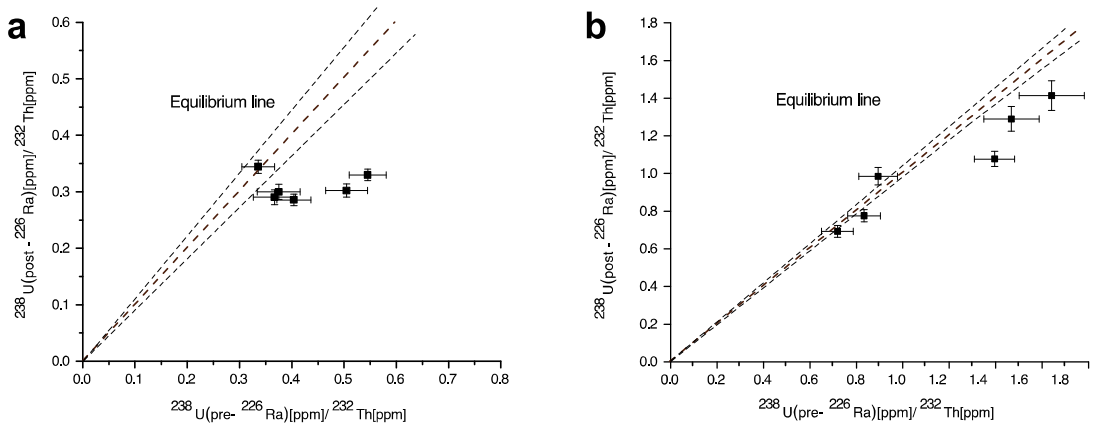

Figure 5. Evaluation of the disequilibrium in the decay chain of ^{238}U for determined dose rates series 1 (left) and series 2 (right). The ratios of ^{238}U(post-^{226}Ra)/^{232}Th and ^{238}U(pre-^{226}Ra)/ ^{232}Th are shown for all the samples. The ratios for samples BaYa2 to BaYa6 in series 1 show considerable disequilibria. Series 2 is considered to be in radioactive equilibrium except for BaYa5 and BaYa6.

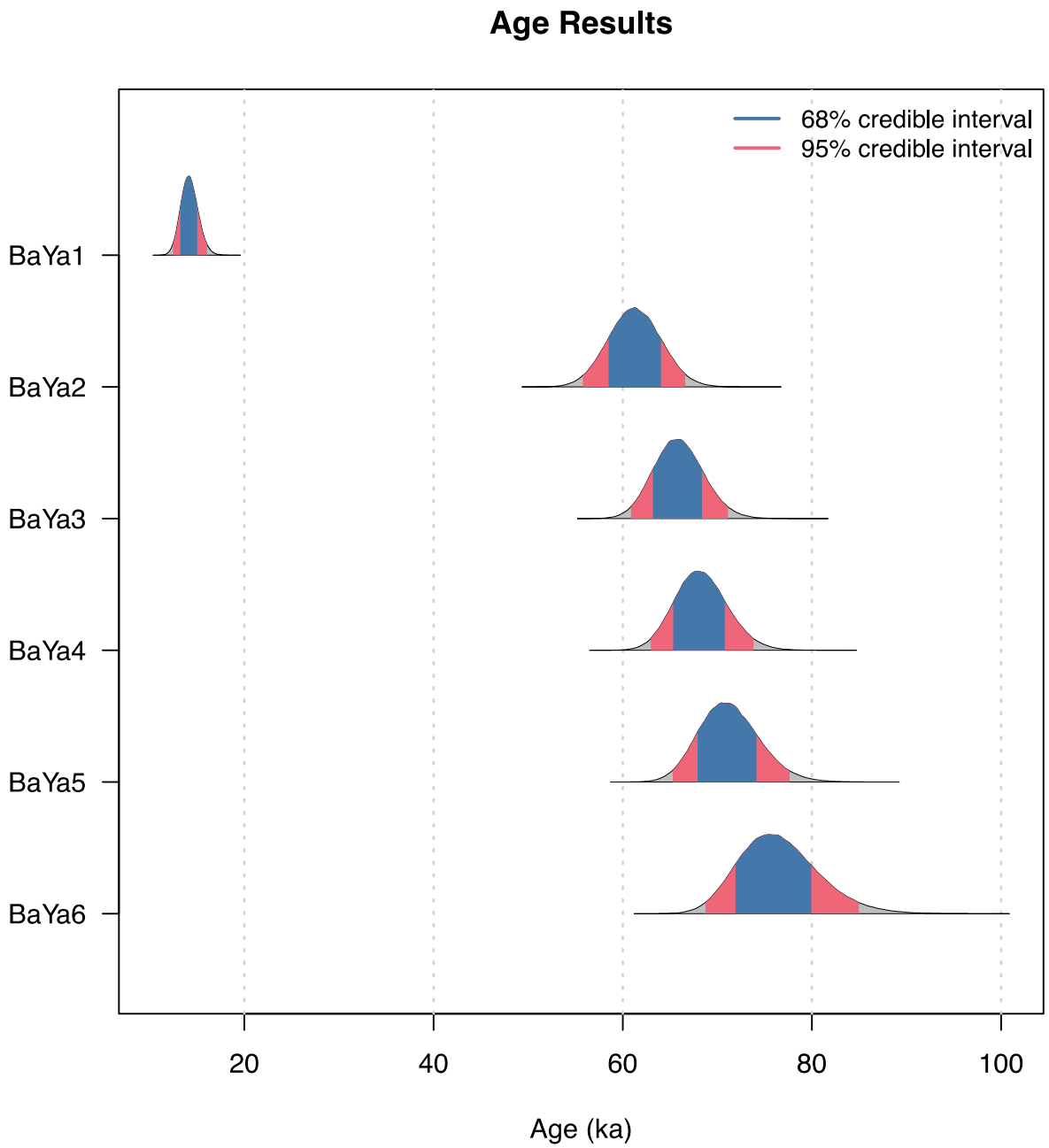

Figure 6. Bayesian posterior age distributions for all six samples. Stratigraphic constraints were included in the modelling. The results are presented with 68% and 95% credible intervals.

Table captions:

Table 1. Radionuclide concentrations of x < 2 mm and 2 mm < x < 1 cm fractions. U top (pre-^{226}Ra) is estimated using the equivalent concentrations of the elements of ^{234}Th, ^{234m}Pa, and ^{234}U. U bottom (post-^{226}Ra) is ascertained from ^{214}Pb and ^{214}Bi at the bottom of the chain.

Sample names	K (%)	σ	U top (ppm)	σ	U bottom (ppm)	σ	Th (ppm)	σ
X < 2 mm fraction								
BaYa1	1.57	0.02	2.23	0.10	2.28	0.03	6.63	0.07
BaYa2	1.46	0.03	2.52	0.13	2.01	0.03	6.71	0.09

BaYa3	1.42	0.03	2.41	0.13	1.91	0.03	6.47	0.09
BaYa4	1.73	0.03	3.91	0.15	2.34	0.04	7.75	0.10
BaYa5	1.99	0.03	3.73	0.15	2.63	0.04	9.22	0.10
BaYa6	1.85	0.03	4.79	0.15	2.90	0.03	8.78	0.09
2 mm < x < 1 cm fraction								
BaYa1	0.52	0.01	2.09	0.09	2.30	0.03	2.34	0.05
BaYa2	0.83	0.02	2.83	0.12	2.72	0.04	3.93	0.07
BaYa3	0.84	0.02	3.07	0.12	2.86	0.04	3.68	0.06
BaYa4	0.51	0.02	3.38	0.11	2.97	0.04	2.30	0.05
BaYa5	0.47	0.02	3.61	0.13	3.11	0.04	2.20	0.05
BaYa6	0.64	0.01	4.22	0.11	3.25	0.03	3.02	0.05

Table 2. The alpha (for quartz and polymineral), beta, gamma, and cosmic dose rate estimates for all samples. $Alpha_Q$ and $Alpha_{PM}$ refer to alpha dose rates estimated for quartz and polymineral, respectively.

Sample name	$Alpha_Q$ (Gy/ka)	σ	$Alpha_{PM}$ (Gy/ka)	σ	Beta (Gy/ka)	σ	Gamma (Gy/ka)	σ	Cosmic (Gy/ka)	σ
BaYa1	0.13	0.02	0.42	0.03	1.35	0.10	0.70	0.02	0.24	0.02
BaYa2	0.13	0.02	0.40	0.03	1.31	0.10	0.73	0.02	0.20	0.02
BaYa3	0.12	0.02	0.37	0.03	1.26	0.10	0.70	0.02	0.18	0.02
BaYa4	0.15	0.02	0.45	0.03	1.45	0.12	0.76	0.03	0.17	0.02
BaYa5	0.17	0.02	0.52	0.04	1.65	0.14	0.86	0.04	0.16	0.02
BaYa6	0.17	0.02	0.53	0.04	1.61	0.14	0.86	0.04	0.15	0.02

Table 3. Summary of quartz OSL and polymineral $pIRIRSL_{290}$ D_e values, dose rates (D_rs), and the relative ages (the uncertainties are presented within 1σ) using the software "Analyst". Bayesian ages using "BayLum" for quartz samples are shown with 68 % credible interval.

	Quartz OSL						Polymineral $pIRIRSL_{290}$						Bayesian Quartz OSL
Sample name	D_e (Gy)	σ	D_r (Gy/ka)	σ	Age (Ka)	σ	D_e (Gy)	σ	D_r (Gy/ka)	σ	Age (ka)	σ	Age (ka)
BaYa1	34	1	2.43	0.11	14	1	50	1	2.82	0.11	18	1	[13-15]
BaYa2	139	3	2.37	0.10	59	3	168	3	2.75	0.11	61	3	[58-64]
BaYa3	154	5	2.26	0.10	68	4	168	4	2.62	0.11	64	3	[63-68]
BaYa4	164	6	2.52	0.13	65	4	181	3	2.94	0.13	62	3	[65-71]
BaYa5	195	6	2.84	0.15	69	4	242	8	3.30	0.15	73	4	[68-74]
BaYa6	204	7	2.79	0.14	73	5	259	8	3.26	0.15	79	5	[72-80]